Uniaxial Magnetic Anisotropy Energy of Fe Wires Embedded in Carbon Nanotubes

Francisco Muñoz,[†,‡] Jose Mejía-López,[†,‡] Tomas Pérez-Acle,[§] and Aldo H. Romero*[,⊥]

[†]Facultad de Física, P. Universidad Católica de Chile, Casilla 306, Santiago, Chile, [‡]Centro para el Desarrollo de la Nanociencia y la Nanotecnologia CEDENNA, Avda. Ecuador 3493, Santiago, Chile, [§]Departmento de Ciencias de la Computación, Facultad de Ingeniería, P. Universidad Católica de Chile, Casilla 306, Santiago, Chile, and [⊥]Materials Department, CINVESTAV, Unidad Querétaro, Libramiento Norponiente 2000, Real de Juriquilla, CP 76230, Querétaro, QRO, México

ABSTRACT In this work, we analyze the magnetic anisotropy energy (MAE) of Fe cylinders embedded within zigzag carbon nanotubes, by means of *ab initio* calculations. To see the influence of the confinement, we fix the Fe cylinder diameter and we follow the changes of the MAE as a function of the diameter of the nanotube, which contains the Fe cylinder. We find that the easy axis changes from parallel to perpendicular, with respect to the cylinder axis. The orientation change depends quite strongly on the confinement, which indicates a nontrivial dependence of the magnetization direction as function of the nanotube diameter. We also find that the MAE is affected by where the Fe cylinder sits with respect to the carbon nanotube, and the coupling between these two structures could also dominate the magnetic response. We analyze the thermal stability of the magnetization orientation of the Fe cylinder close to room temperature.

KEYWORDS: carbon nanotubes · magneto-anisotropy · magnetic arrangement · encapsulated metal nanowires

The use of cylinder nanostructures have found widespread set of potential applications, which include medical, optical, electronic, and magnetic. In the past few years, ferromagnetic nanowires (NW)[1−6] and carbon nanotubes (CNT) filled with a ferromagnetic metal or even monocrystal NW (NW + CNT) has been widely studied and characterized.[7−11] In particular, it has been discussed in the literature that 1D magnetic nanostructures can be extensively exploited for their potential uses in ultrahigh-density magnetic storage devices.[5,12−14] This type of patterned array has been suggested to have a large impact as recording media, because it could achieve a very large recording density, between 100 Gbit/in^2 and 0.4 Tbit/in^2, in the case of ferromagnetic NWs[15,16] and in the case of metallic NW + CNTs, it could be up to 1 Tbit/in^2.[8] The latter systems have some advantages over a ferromagnetic metal NW: their synthesis process allows a higher density and the carbon coat can prevent them from oxidation (which can turn the NW into an antiferro or ferrimagnetic material).[8]

For magnetic recording media detailed knowledge of magnetic anisotropy is important. The presence of the magnetic anisotropy in a crystalline system prevents a spontaneous change in the magnetization direction (*i.e.*, bit changes from "0" to "1"). The magnetic anisotropy energies arise mainly from two sources: the first is the interaction energy between magnetic dipoles (*i.e.*, the atomic spin), and the second, called magnetocrystalline anisotropy energy (MAE), comes from the coupling between the magnetic moment and the crystal field. Finally, lattice distortions can change both anisotropy energies and could also give rise to some additional anisotropy.

The dipolar anisotropy, also called shape anisotropy, is determined by the system shape, and it comes from the alignment of the atomic magnetic moments along the vector joining them.[17] In a magnetic NW, this anisotropy usually is very strong (dominant) and the easy axis corresponds to the wire symmetry axis.[3,4] As a consequence, the hysteresis loop of a magnetic NW has a square-like shape with high coercivity. This physical observation strengthens the potential to use them in nanodevices, where having a monodomain is of vital importance, which is the case when the NW length scales are smaller than the domain length.[1] For a bulk system, such as bcc iron, this anisotropy term is normally negligible, compared with other energies present in the system. On the other hand, when the NW area density is high, the dipolar contribution between different wires is no longer small and competes with the anisotropy of a single nanowire. Encinas *et al.*[18] have shown that in arrays of nickel nanowires, even the easy axis changes from parallel to perpendicular to the NW when the porosity

*Address correspondence to aromero@qro.cinvestav.mx.

Received for review December 15, 2009 and accepted April 19, 2010.

Published online Xxxxxxxxx 00, 0000
10.1021/nn901834z

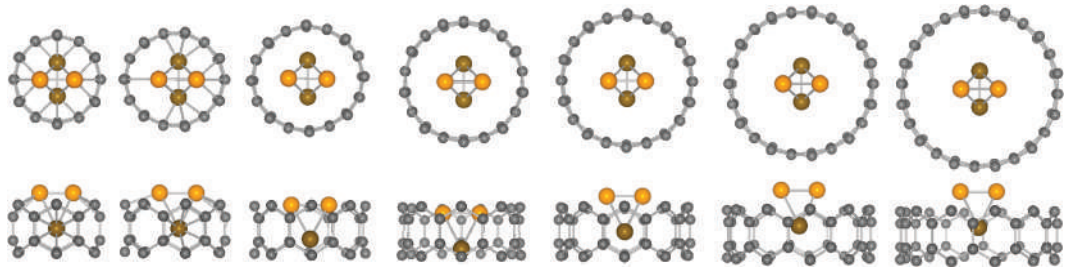

Figure 1. Fe NW inside zigzag carbon nanotube relaxed structures. From left to right: (6,0), (7,0), (8,0), (9,0), (10,0) (11,0), (12,0) CNT. The color on Fe atoms indicate its layer position. Bottom figures show corresponding lateral view of the unit cell.

of the template (in which the NWs have been grown) reaches a critical value, that is, the dipolar anisotropy is too small to keep the magnetization along the NW axis.

The other anisotropy source is the MAE, which arises from the spin−orbit coupling, that is, the coupling between the electrons spin and the lattice. In bulk systems, the MAE tends to be small, the lattice high symmetry (usually cubic) cancels the lower order contributions. The MAE has been the subject of a large body of studies in bulk and two-dimensional systems (*i.e.*, interfaces and films).[19−28] The MAE becomes quite competitive, or dominant, when the dipolar interaction is small, as in dense packed Ni NW (see above), or it can also be greatly enhanced, when the system symmetry is decreased. For instance, Hjortstam *et al.*[19] have studied how the face-centered-tetragonal bulk Ni (*i.e.*, modified by an external stress), can yield a MAE even orders of magnitude greater than fcc Ni. Also, very large MAE has been recently reported in low dimensional systems such as monatomic Co NWs, where it was found that the MAE is the main contribution to the magnetic state.[6]

In the following sections, we present a study of the MAE of pristine Fe NW and also Fe NWs embedded into single wall CNTs, by using density functional theory. We discuss our computational approach and we analyze the ground-state structures. We then show the MAE for the lowest energy structures and gives a discussion of the observed behavior. Finally we show the behavior of the MAE at room temperature. We conclude this paper by outlining our conclusions and perspectives.

RESULTS AND DISCUSSION

Structural Relaxation. To see the effects of confinement on Fe cylinders, we have chosen to study the zigzag CNT, because it is a good match with the lattice parameter of Fe bcc (110),[10] which prevents the appearance of effects coming from local strains. Our systems are constructed by placing a Fe NW (always the same NW) inside a CNT, and then letting the system relax until the forces on each ion are negligible. We have carried out this procedure by considering several nonequivalent configurations, that is, different azimuthal angles between both structures as well as different translations along the symmetry axis, as seen in Figure 1. Herewith, only the lowest energy configurations are reported. We found that for most cases, these structures correspond to the case where the NW and CNT symmetry axes coincide, except for the CNT (7,0), as can be observed in Figure 1 and Figure 3.

To study the effect on the structural and energetic properties of the Fe NW when it is embedded within the carbon nanotube, we find it useful to define the following energies:

$$E_b = (E_{system} - E_c N_c - E_{Fe} N_{Fe})/(N_c + N_{Fe}) \quad (1)$$

$$E_{iron} = (E_{system} - E_{CNT} - E_{Fe} N_{Fe})/N_{Fe} \quad (2)$$

where E_b is the binding energy, which depends on the total system energy, the energy of isolated carbon and Fe atoms (E_c and E_{Fe}, respectively) and their corresponding number of atoms within the system, while E_{iron} measures the binding energy of the Fe NW with respect to the carbon nanotube (E_{CNT} is the energy of the pristine CNT).

Table 1 summarizes the energies obtained from eqs 1 and 2. The binding energy (E_b) is always negative, which demonstrates that all considered structures are energetically stable, and its value increases as a function of the N_C/N_{Fe} ratio (which coincides with the first CNT index). E_{iron} is just the binding energy of Fe atoms belonging to the Fe NW, when the whole Fe cylinder is embedded within the carbon nanotube. From this energy, it can be seen that, with CNTs ranging from (8,0) up to

TABLE 1. Binding Energies E_b and E_{iron} (in eV and as Defined in eqs 1 and 2), Magnetization by Magnetic Atom (in μ_B), Average Nearest C−Fe Distance (in Å), and Ratio between the NW Diameter with Respect to the CNT Diameter

structure	E_b	E_{iron}	Mag/Fe	$d_{C\text{-}Fe}$	D_{NW}/D_{CNT}
NW isolated	−2.9	−2.9	3.19		
NW + (6,0)	−6.7	−1.6	0.88	2.03	0.39
NW + (7,0)	−7.0	−2.5	1.54	2.24	0.36
NW + (8,0)	−7.2	−2.9	2.73	2.50	0.34
NW + (9,0)	−7.3	−3.0	2.87	2.84	0.31
NW + (10,0)	−7.4	−2.9	2.79	3.25	0.27
NW + (11,0)	−7.4	−2.9	3.07	3.62	0.25
NW + (12,0)	−7.5	−2.9	3.17	3.97	0.23

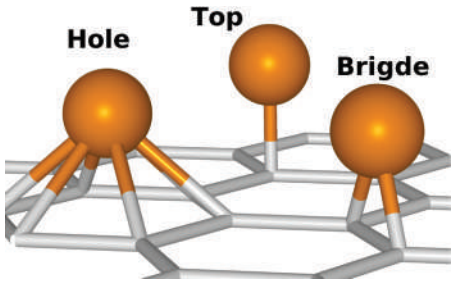

Figure 2. Possible adsorption sites for a single Fe atom inside a CNT as considered in ref .

(12,0), the system can be energetically regarded as a confined NW and a free CNT. In the case of smaller CNTs, the Fe atoms are less bound in the NW+CNT system than in the isolated NW, but the lowest energy structure coincides with the case where the Fe NW and the carbon nanotube fits the best. Only, when the Fe NW is embedded within (11,0) and (12,0) CNTs, we observe that the magnetization is quite similar to the isolated NW case, which indicates that below a diameter ratio of 0.25 (between the NW and the CNT), the carbon nanotubes do not have any influence on the electronic and magnetic properties of the Fe NW.

With respect to the ground state geometries, we should note that as the CNTs gets thinner, the Fe NW will have less space to accommodate and it has to find an optimal configuration. It was already pointed out by Yagi *et al.*,[29] that an adsorbed Fe will sit in the middle of the carbon hexagon (see the "hole" position in Figure 2). This implies that as the number of Fe atoms is increased, the Fe NW is forced to accommodate within the carbon nanotube hexagons. Therefore, the optimal configuration will be when most of Fe atoms are in those hexagonal positions. On the other hand, for the NW geometry we have considered, there are only few cases where there is a maximum number of Fe atoms sitting in the middle of the carbon hexagons. Those happen for carbon nanotubes with indices $(4n + 2, 0)$, $n = 1, 2, \ldots$ (for example the case of NW + (6,0) in Figure 1). Instead, in the case of a NW + (7,0), while one Fe atom could be facing a carbon hexagon, the opposite one within the same layer on the NW cylinder can only be in a bridge type of position (Fe atoms within the same layer have the same color in Figure 1) and can be only in front of a C−C bridge due the lack of reflection symmetry of (7,0) CNT. Therefore, to decrease the energy of such a configuration, a translation between the CNT and the Fe NW axes needs to be performed, such that three Fe atoms are in a hexagonal position while only one is in a bridge position. This transformation changes the CNT from cylindrical to elliptical. Similar reasoning can be applied to other cylinders where the carbon nanotube does not have the $(4n + 2, 0)$ index.

Figure 3 shows the electronic charge density for some of the Fe NW + CNTs systems considered here.

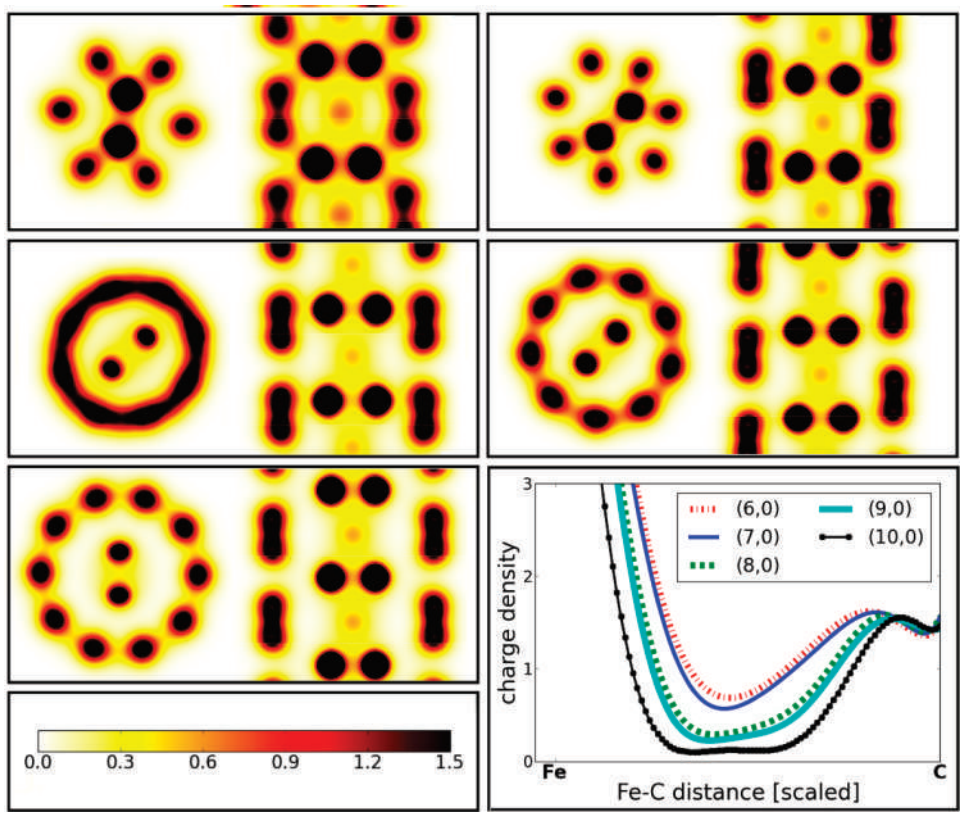

Figure 3. Charge density (top and laterals views), from top left: NW + (6,0), NW + (7,0), NW + (8,0), NW + (9,0), NW + (10,0). The same color scale (at bottom) is used for all structures. The last picture is the charge density between an Fe and a C atom. All distances are scaled to fit the same area.

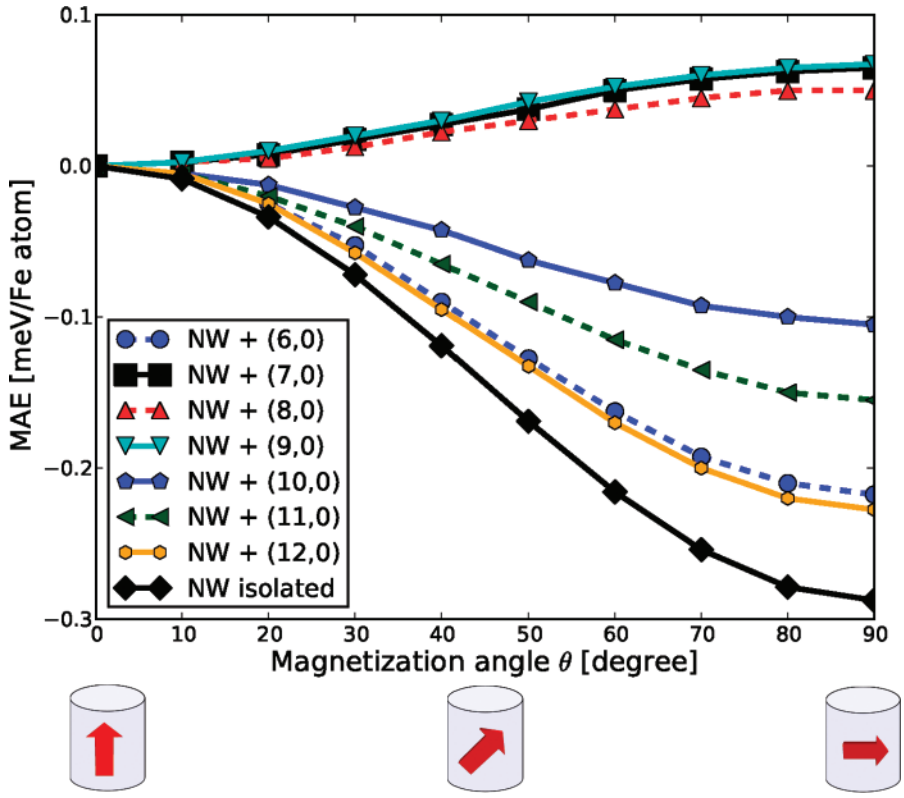

Figure 4. MAE as a function of magnetization angle. A minimum in 0° means the easy axis parallel to NW axis.

In this figure, all the 2D planes pass through the middle of a pair of neighbor Fe atoms, where the top view also is perpendicular to the CNT axis and the lateral view passes through the NW center. The electronic charge density demonstrates that NW + (6,0) and NW + (7,0) systems have a strong interaction between the two coupled systems, where there is a non-negligible charge distribution between the NW and CNTs. Only in the case of NW + (10,0), is the charge overlap negligible. It is also clear in the NW + (8,0) case that the belt electronic charge comes from the C σ-bonds. We also note the metallicity of the NWs seen in all the images. We have completed this analysis by looking at the electronic localization function (ELF), and we notice a clear electronic distribution on the Fe atoms and C atoms, with greater contribution to the ELF in the NW + (6,0) and NW + (7,0) cases. This contribution decreases as the CNT increases its diameter, while in the space between both substructures the ELF tends to zero faster when the CNT increase its diameter. The magnetization is mostly localized on the Fe atom with a very tiny contribution (less than 2%) from the carbon atoms.

Magnetocrystalline Anisotropy. Nanowires and nanotubes can be regarded as prototypical one-dimensional structures, so the most interesting questions with respect to the magnetic configuration can be spelled as: Is the easy axis parallel or perpendicular to the nanotube axis? Can the CNT modify the anisotropy value or orientation? To answer these questions, first we check how large is the MAE within the plane perpendicular to the structure axis. It is expected that anisotropies on the plane are smaller than those along the axial axis, and hence they should be reflected in the calculations and used as evaluation of its quality. Our results indicate that there is no significant change in energy on the perpendicular plane to the axial axis. Even though we did test on selected structures, such as an isolated NW and a NW + (6,0), we consider this observation general for the other NW + CNTs. Of course, our calculations do not discard a small MAE in this plane, but we can safely ignore it, especially if the in-plane anisotropy is compared to the one obtained by considering the magnetization along the perpendicular and the axial axis, which happens to be at least 2 orders of magnitude larger.

Next, we perform calculations of the total energy while rotating the magnetization angle from parallel (zero-degrees) to perpendicular (ninety-degree) with respect to the structure axis, within 10 degree intervals and using the following MAE definition:

$$\mathrm{MAE}(\theta) = E(0^{\circ}) - E(\theta) \qquad (3)$$

where θ is the magnetization angle measured from the CNT axis ($\theta_{\mathrm{parallel}} \equiv 0°$). MAE(90) is the anisotropy between the two relevant orientations, which is the value usually reported in the literature. Figure 4 summarizes our measured MAE(θ), as a function of rotation angle.

Surprisingly the questions stated above are tightly entangled: the easy axis depends strongly and non-monotonously on the CNT index. There exist two

TABLE 2. Anisotropy Constant K_1 per Fe Atom

structure	K_1 (meV)
NW isolated	−0.29
NW + (6,0)	−0.22
NW + (7,0)	0.07
NW + (8,0)	0.05
NW + (9,0)	0.07
NW + (10,0)	−0.10
NW + (11,0)	−0.15
NW + (12,0)	−0.23

marked trends: On one side the easy axis of an isolated NW is perpendicular to its NW axis, and for the nanowire embedded into "large" nanotubes, (10,0) or bigger, the system gradually starts behaving as a free NW. On the other hand, if the NW is more confined (CNT (7,0) to (9,0)), the interaction with the carbon nanotube induces a different MAE about five times smaller than that in the free NW, where the easy axis is along the structure axis. The NW + (6,0) does not follow this trend mainly because the NW is more confined and there is a large change on the magnetization value with respect to the free NW (see table 1). We think that this particular case can be explained on the basis of symmetry arguments. Among all the geometries we have considered, this is the only case where the NW + CNT nanostructure remains very close to the symmetry of the isolated NW. The metallic NW is not structurally modified after confinement. Therefore, the confinement only affects the electronic states and increases the gap between them as well as the electronic localization (see Figure 3).

The results shown in Figure 4 can be used to obtain the anisotropy constant, which in a system with a given axial symmetry is defined as

$$E(\theta) = \sum_{N=0}^{\infty} K_N \sin(\theta)^{2N} \qquad (4)$$

Mainly because of symmetry constraints, the expanded contribution from the MAE in our case reduces to $K_1 \sin^2(\theta)$, becoming dominant, while a fitting procedure shows that higher contributions are vanishing. The anisotropy constants from eq 4 are reported in Table 2, where a positive value means that the easy axis is parallel to the structural axis. We can see that these values are 3 orders of magnitude larger than the anisotropy constant of the bulk Fe. It is noteworthy that the reported value of the MAE for a monatomic Co chain is an order of magnitude larger ($K_1 = 2.0$ meV/atom)[6] than that calculated here, and is also 3 orders of magnitude larger than the bulk Co. In particular, physical parameters such as MAE or the exchange coupling constant appear naturally in describing magnetic systems by model Hamiltonians, which implies that those parameters need to be obtained from more accurate calculations or by relating some observables to experimental measurements. For instance, ref 30 uses model Hamiltonians to shown how the magnetic stability of magnetic nanotubes depends quite strongly on the magnetocrystalline anisotropy. Therefore, implications on the magnetic properties of the confinement are noticeable also from Hamiltonian models.

In a 1D case, we find that the mechanism responsible for the change of the magnetization direction as a function of the CNT index is mostly due to NW + CNT symmetry breaking. To clarify this observation and the magnetization dependence on the symmetry, we artificially rotate the NW around its axis by an angle α, where the CNT structure is kept fixed (see Figure 5). Even though we recognize that these configurations happen to be energetically unstable, we should point out that the aim of this exercise is not the feasibility of other structures, but learning about the MAE dependences with respect to changes in symmetry.

As it has been already discussed, the NW + CNT with the largest magnetic differences with respect to the Fe NW is the (6,0) (see Figure 4). Hence, we now focus on this case. This joint system, NW + CNT, has a plane periodicity of 60°, which indicates that it is only necessary to measure the MAE within the range 0°−30°. Figure 5 shows some geometrical configurations used in our calculations, where now MAE(90°) $\equiv E_{\text{parallel}} - E_{\text{perp}}$ is the one reported in Figure 6.

The changes on the MAE as a function of the rotation angle, meaning a change of relative symmetry between the two systems (Fe NW and CNT), is reported in Figure 6. The changes in energy are related to how the Fe atoms sit with respect to the carbon hexagons in the nanotube. For example, it has been proposed that changes in MAE (in Fe/ZnSe) are due to anisotropic interfacial bonds; that is, at the interface, two different types of Fe exist due to a different set of second neighbors.[24] It also seems to be the case in the NW + CNT

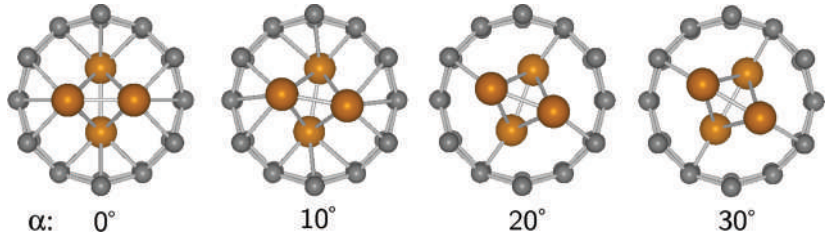

Figure 5. An imposed rotation on the Fe NW around its axis within a (6,0) carbon NT. The number corresponds to the rotation angle α, measured from the ground-state

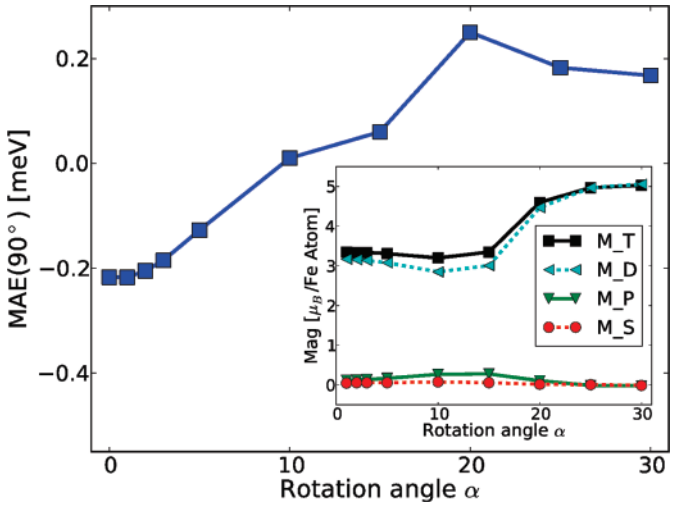

Figure 6. MAE(90°) for Fe NW axially rotated in a fixed (6,0) carbon nanotube. The rotation angle is measured with respect to the ground state configuration. The inset shows the total and s, p, d orbital projections to the magnetization for the considered structures.

system. To take a look at the bonds, we can now refer to Figure 7, in which the electronic charge density of some of the considered nanostructures is shown, with the free atomic density subtracted from the total electronic density. This is a good guess of the overlap charge density. Figure 7 shows clear differences between the charge distributions. We note two remarkable features: First, in the case of $\alpha = 0°$, the charge on each iron atom appears as bright yellow dipoles. The NW charge difference is less localized near the nuclei and spreads mostly around the NW, mainly between the Fe−Fe bonds and the C−C π-orbitals. When the rotation angle takes the values of $\alpha = 20°, 30°$, the transferred charge near the Fe atoms has a quadrupole pattern. The density along the carbon NT atoms is mostly localized with a small contribution from π-orbitals. In the case of an angle of rotation of $\alpha = 10°$, both electronic density distributions are mixed, which balances all different electronic asymmetries, giving a null MAE. Second, from the calculations of the different orbital contributions to the magnetization (inset in Figure 6), it is clear that M_d and M_p have opposite trends: the maximum (minimum) of M_d (M_p) is at $\alpha = 30°$ and its minimum (maximum) for α is equal to 10°.

In the case of $\alpha = 0$, we can identify two types of different carbon atoms by how they interact with the Fe atoms, due to the different distance between the carbon atom and the closest Fe atoms. Both are noted in Figure 8, where we used different colors to identify the carbon type in the carbon nanotube. After a small rotation of 10° is applied into the Fe NW, the interaction between Fe and C atoms is modified, and now we can identify three different types of carbon atoms, which have different distances between Fe and C (see Figure 8). This geometrical identification can also be observed from the density of states, where the contribution from p_z orbitals for each nonequivalent type of C atom is reported. As discussed in ref 24, the MAE is mostly due to this bonding anisotropy.

Thermal Stability. As stated in the introduction, these 1D systems are promising candidates for recording media, and it is important to know how much the MAE fluctuates as a function of temperature. These potential changes arise from the coupling between the electronic structure and the phonons excited at that given temperature, especially in those vibrations where there is a clear change in the symmetry. To simulate the effect of temperature, we perform *ab initio* molecular dynamics simulations (MD) for three cases: an isolated NW, NW + (6,0) and NW + (7,0). These systems were selected because each represents a different case: the isolated NW would loose its symmetry with the temperature but obviously without interacting with a C atom. The NW + (6,0) would loose its symmetry giving rise to anisotropic Fe−C bonds, which can affect the MAE enormously, as discussed above. Finally, NW + (7,0) has C atoms with different neighborhoods which create a diversity of Fe−C bonding distances. Therefore, temperature can affect not only those C−Fe distances but also the distribution of the different carbon types which can modify the magnetic properties of the whole system. The molecular dynamics simulation was performed by using a spin-polarized calculation to describe the electronic structure and at ~300 K, using a Nosé thermostat[31] (*i.e.*, a thermal bath to simulate the canonical ensemble) with a time step of 1 fs and a total simulated time of 310 fs. Because of the simplicity of our systems the relaxation is almost immediate and our simulation time is enough to take a clear look of what happens with the MAE. During the time evolution, frames were obtained every 10 MD steps and calculations for all extracted configurations were performed.

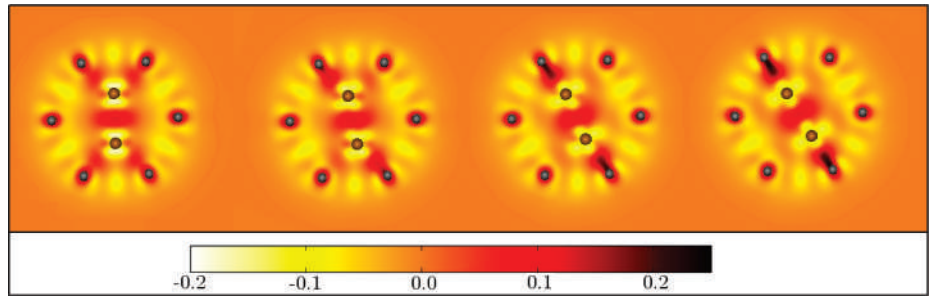

Figure 7. Difference between the total and atomic electronic charge densities. From left to right $\alpha = 0, 10, 20, 30$.

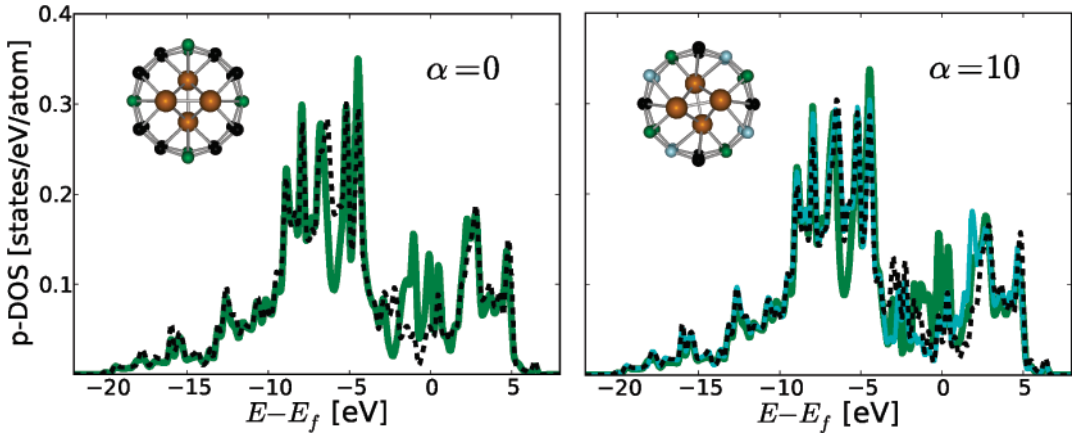

Figure 8. Density of states for p_z orbitals of C atoms; each color represents a nonequivalent type of C.

First of all, for a specific frame, the wave function and charge density were calculated (spin-polarized and collinear) with high accuracy, spins were rotated toward the desired directions, and the corresponding energies or the MAE was calculated. An average was obtained from all MAE calculations for all considered frames.

Shown in Figure 9, are the average MAE(90°) and the average magnetization with the error bars due to the standard deviation at the predefined temperature. From this figure, we can conclude that the MAE for the isolated NW remains quite close to the zero temperature value, which means that the anisotropy of the Fe−Fe bonds plays almost no role in changing the MAE. But when the NW is embedded into the (6,0) CNT, the situation changes radically, the MAE dispersion increases by almost two orders of magnitude. This observation confirms our finding that the anisotropic bonding of Fe atoms with the carbon atoms on the nanotube is responsible for the intrinsic changes of the MAE. As expected, the easy axis of NW + (7,0) is still parallel to the structure axis, but its MAE increases by about 30% (with respect to the ground state), and it has little fluctuations around its mean value at room temperature. This is because the temperature can enhance the anisotropy of Fe−C bonds by giving the necessary energy to move the Fe atoms from the optimal position in front of the C hexagons (see Figure 2). Also in this last case, the average magnetization per atom is 0.1 μ_B greater than that in the ground state structure (in all other cases it is nearly the same). The simulation also shows that the MAE is weakly related to changes on the total magnetization, for example, in the case of NW + (6,0), where there is a large ionic displacement, the change of the MAE is noticeable which is not the case for the magnetization, which remains almost constant.

Finally, Figure 9 also reports the results of our calculations performed at zero temperature on the NW + CNT by applying a uniform strain of 2% along the CNT axis. As expected, it produces rather small changes in the MAE, but with a clear tendency to lower its value (i.e., if the easy axis is perpendicular to the CNT this means an increase in MAE magnitude). Therefore, changes on the system strain are not able to enhance the MAE as it can be obtained by temperature, at least for well coupled NW + CNT.

Nevertheless, it is important to recall that only a few CNTs can have symmetric matching with the considered NW, in our case only (6,0), (10,0), *etc*. So, in a general case, arrays of Fe-filled CNTs would have the easy axis parallel to the structure axis with a large MAE of ~0.1 meV/Fe atom. The temperature (at least up to room temperature) would only increase the MAE value. Hence this expected general case can be useful for longitudinal magnetic recording media using each CNT as a monodomain. We should also point out that in thicker NWs, where the number of Fe atoms without direct interaction with the CNT is larger, the dependence could be different from the one studied here.

CONCLUSION

We have confirmed the geometrical stability of small Fe cylinders within carbon nanotubes, as it was discussed in ref 10. By using these optimized geometries, we were able to identify the effect of confinement on magnetoanisotropy energies. We report that the most stable configurations are obtained when there is a perfect matching between a CNT and a Fe NW, which is the

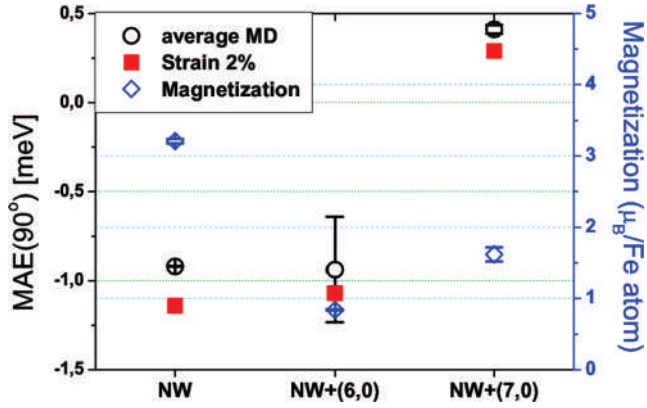

Figure 9. Average MAE(90° (left axis) and magnetization (right axis) at room temperature. The error bars show the standard deviation over the considered sampling.

case when a large number of Fe atoms are in front of carbon hexagons. For this particular case, the effect of confinement provided by the CNT on the MAE is much lower than in other cases. Depending on how the NW sits inside the CNT or more specifically if the CNT + NW system preserves (or lowers) the symmetry of the isolated NW, the easy axis can be perpendicular (parallel) to the CNT axis, with a MAE magnitude of around 0.2 meV (0.06 meV) per magnetic atom. The magnetoanisotropy energy as function of the magnetic moment direction can be described by a second order expansion and with an anisotropy constant quite dependent on the Fe NW confinement. We demonstrate that the physical mechanism that relates the MAE change and the breaking of symmetry in the Fe NW is the creation of anisotropic Fe−C bonds (*i.e.*, inequivalents types of C when they bind to Fe atoms). The direction of the MAE can be manipulated by different means and it is dependent on how changes to the interface between Fe atoms and the CNT are made. We also studied the possible changes of the MAE as a function of temperature and strain. For that, we considered three different cases, where the effect of confinement goes from no change of the magnetic properties of the Fe NW up to a large modification (up to 30%).

We find that at room temperature, the MAE fluctuations of pristine NW are small in relation to atomic vibrations, for CNT + NW with asymmetric matching, such as NW + (7,0), the MAE not only keeps favoring a parallel alignment also increases its value. Finally when the CNT + NW forms symmetric bonds (which give them a perpendicular easy axis), these bonds are distorted by atomic vibrations greatly lowering the MAE magnitude.

METHOD AND COMPUTATIONAL DETAILS

The system here considered has been built from a small Fe NW embedded within a zigzag CNT (i,0), with the index i = 6, 7, 8, 9, 10, 11, 12. The Fe NW has been created from (011) bcc iron, which guarantees an almost perfect match between the two different cell parameters (the mismatch is around 5%). Wave functions are expanded in plane waves by using the Bloch theorem, which makes the wire infinite along the wire axis. Therefore, to avoid interaction between neighbor cells perpendicular to the NW axis, a large vacuum slab (at least 10 Å) was considered to avoid spurious interactions between periodic images. Despite our structures being "isolated" from electronic interactions (short ranged, which are only of few angstroms), our results are also valid for somewhat dense NW arrays in which the dipolar interaction is small (as the cases discussed on the introduction[8,18]). The considered structures within this study are shown in Figure 1, where for completeness, the isolated NW was also simulated and taken as a reference.

We perform a density functional theory study (DFT) as implemented within the VASP code[32−35] with projector augmented waves (PAW) pseudopotentials[36,37] and a generalized gradient approximation due to Perdew, Burke and Ernzerhof (PBE) for the exchange correlation.[38] From an experimental point of view, the magnetocrystalline anisotropy is obtained after the demagnetization energy is subtracted from the measurements ($-\pi\mathbf{M}^2$), while, from the theoretical point of view, this subtraction is not necessary because the MAE is obtained directly from the total energy.

For all structures considered here, we first performed a careful ionic relaxation until forces were negligible, $|\mathbf{F}| < 0.01$ eV/Å. We tested that a tighter precision on forces would not produce any noticeable improvement on the total energies. During the ionic optimization, the cell parameter along the cylinder axis was kept constant at 4.26 Å, while the perpendicular directions were at least 10.0 Å plus the nanotube diameter.

With respect to the magnetic configuration, we only considered a ferromagnetic orientation, because it is the ground-state for an isolated Fe NW and it should also be the case for the NW + CNT.[7,10] After the total energy minimization, the wave function and density were minimized under the assumption of collinearity and without considering the spin−orbit coupling. These quantities serve as input for the following step. This last step corresponds to a noncollinear non-self-consistent calculation, where the spins were oriented toward the desired crystal direction and the spin−orbit coupling correction was included,[39] in particular, the ferromagnet NW orientation was given along the nanowire axis. Under those assumptions, the total energies were calculated. We used a convergence criterion of 10^{-7} eV in both self-consistent and non-self-consistent loops. Even though we have obtained the prescribed convergence with only 10 K-points, we have used a larger number to improve the description on the band energies. In particular, we have used 100 points for the smaller structures, while we have used 30 for the largest ones ((10,0), (11,0), and (12,0)). To test the aforementioned method, we have performed fully self-consistent calculations, for specific cases, where the spin−orbit coupling was considered from the starting geometrical optimization. The MAE agrees with both cases, and we decided to proceed with the first method to avoid time-consuming calculations.

The tight convergence of the total energy is an important requirement to calculate tiny values corresponding to the MAE. For reference, the MAE is of the order of approximately μeV in bulk systems,[21,23,36] and for surfaces and thin films its magnitude increases to approximately meV.[19,20,22,24,27] To have a clear convergence on the physical quantities of interest, a very large k-mesh is also necessary. For example, it has been reported that for MAE in bulk systems, a huge number of k-points was required (*ca.* 10^4-10^5),[21] while for surfaces and 2D systems the convergence in k-space is achieved with only *ca.* 10^4 or 10^3 points.[19,20,24] For our system, which corresponds to a 1D periodicity, the convergence is achieved more easily, and even with 10 k-points the energy only changes within the fifth digit. But, to ensure the quality of our results and makes them independent of the mesh we have used a very dense mesh.

Acknowledgment. J.M. and F.M. acknowledge support from Vicerectoría Adjunta de Investigación y Doctorado-PUC under the project Límite #06/2009, the Millennium Science Nucleus, Basic and Applied Magnetism Grant No. P06-022F and the project Financiamiento Basal para Centros Científicos y Tecnológicos de Excelencia. F.M. also thanks the Doctoral Fellowship from Conicyt. T.P.A. thanks ACTION-Grid project, Support Action 224176 for European Economic Community FP-07 International Cooperative Action on Grid Computing and Biomedical Informatics between the European Union, Latin America, the Western Balkans and North Africa, Programa de Financiamiento Basal PFB16, and Fundaci on Ciencia para la Vida. A.H.R. has been supported by CONACyT Mexico under projects J-59853-F, J-83247-F, and TAMU-CONACyT. We thank Prof. Verstraete and Prof. Roshchin for a critical reading of the manuscript, Sinhue Lopez for providing details on how to perform noncollinear magnetic calculations, and F. David for his figures help.

REFERENCES AND NOTES

1. Nielsch, K.; Wehrspohn, R.; Barthel, J.; Kirschner, J.; Gösele, U.; Fischer, S.; Kronmüller, H. Hexagonally Ordered 100 nm Period Nickel Nanowire Arrays. *Appl. Phys. Lett.* **2001**, *79*, 1360–1362.

2. Lee, G.; Huh, S.; Jeong, J.; Kim, S.; Choi, B.; Kim, B.; J., P. Processing of Ferromagnetic Iron Nanowire Arrays. *Scr. Mater.* **2003**, *49*, 1151–1155.
3. Cornejo, D.; Padrón-Hernández, E. Study of Magnetization Process in Ordered Fe Nanowire Arrays. *J. Magn. Magn. Mater.* **2007**, *316*, e48−e51.
4. Zhang, X.; Wen, G.; Chan, Y.; Zheng, R.; Zhang, X.; N., W. Fabrication and Magnetic Properties of Ultrathin Fe Nanowire Arrays. *Appl. Phys. Lett.* **2003**, *83*, 3341–3343.
5. Yang, S.; Zhu, H.; Yu, D.; Jin, Z.; Tang, S.; Du, Y. Preparation and Magnetic Property of Fe Nanowire Array. *J. Magn. Magn. Mater.* **2000**, *222*, 97–100.
6. Gambardella, P. Magnetism in Monatomic Metal Wires. *J. Phys.: Condens. Matter.* **2003**, *15*, S2533–S2546.
7. Kang, K.-J.; Choi, J.; Moon, C.-Y.; Chang, K. Electronic and Magnetic Properties of Single-Wall Carbon Nanotubes Filled With Iron Atoms. *Phys. Rev. B* **2005**, *71*, 115441.
8. López-Urías, F.; Muñoz Sandoval, E.; Reyes-Reyes, M.; Romero, A.; Terrones, M.; Morán-López, J. Creation of Helical Vortices during Magnetization of Aligned Carbon Nanotubes Filled with Fe: Theory and Experiment. *Phys. Rev. Lett.* **2005**, *94*, 216102.
9. Ivanovskaya, V.; Köhler, C.; Seifert, G. 3d Metal Nanowires and Clusters Inside Carbon Nanotubes: Structural, Electronic, and Magnetic Properties. *Phys. Rev. B* **2007**, *75*, 075410.
10. Weissmann, M.; García, G.; Kiwi, M.; Ramírez, R.; Fu, C.-C. Theoretical Study of Iron-Filled Carbon Nanotubes. *Phys. Rev. B* **2006**, *73*, 125435.
11. Golberg, D.; Mitome, M.; Müller, C.; Tang, C.; Leonhardt, A.; Bando, Y. Atomic Structures of Iron-Based Single-Crystalline Nanowires Crystallized Inside Multiwalled Carbon Nanotubes as Revealed by Analytical Electron Microscopy. *Acta Mater.* **2006**, *54*, 2567–2576.
12. Chou, S. Patterned Magnetic Nanostructures and Quantized Magnetic Disks. *Proc. IEEE* **1997**, *85*, 652–671.
13. Murphy, C.; Jana, N. Controlling the Aspect Ratio of Inorganic Nanorods and Nanowires. *Adv. Mater.* **2002**, *14*, 80–82.
14. Cordente, N.; Respaud, M.; Senocq, F.; Casanove, M.; Amiens, C.; Chaudret, B. Synthesis and Magnetic Properties of Nickel Nanorods. *Nano Lett.* **2001**, *1*, 565–568.
15. Routkevitch, D.; Tager, A.; Haruyama, J.; Almawlawi, D.; Moskovits, M.; Xu, J. Nonlithographic Nanowire Arrays: Fabrication, Physics, and Device Applications. *IEEE Trans. Electron Dev.* **1996**, *43*, 1646–1658.
16. Li, C.-P.; Roshchin, I. V.; Batlle, X.; Viret, M.; Ott, F.; Schuller, I. K. Fabrication and Structural Characterization of Highly Ordered Sub-100-nm Planar Magnetic Nanodot Arrays Over 1 cm^2 Coverage Area. *J. Appl. Phys.* **2006**, *100*, 074318.
17. Chikazumi, S. *Physics of Ferromagnetism*; Oxford Science Publications: Oxford, 2002; p 7.
18. Encinas-Oropesa, A.; Demand, M.; Piraux, L.; Huynen, I.; Ebels, U. Dipolar Interactions in Arrays of Nickel Nanowires Studied by Ferromagnetic Resonance. *Phys. Rev. B* **2001**, *63*, 104415.
19. Hjortstam, O.; Baberschke, K.; Wills, J. M.; Johansson, B.; Eriksson, O. Magnetic Anisotropy and Magnetostriction in Tetragonal and Cubic Ni. *Phys. Rev. B* **1997**, *55*, 15026–15032.
20. Ravindran, P.; Kjekshus, A.; Fjellvåg, H.; James, P.; Nordström, L.; Johansson, B.; Eriksson, O. Large Magnetocrystalline Anisotropy in Bilayer Transition Metal Phases from First Principles Full-Potential Calculations. *Phys. Rev. B* **2001**, *63*, 144409.
21. Trygg, J.; Johansson, B.; Eriksson, O.; Wills, J. M. Total Energy Calculation of the Magnetocrystalline Anisotropy Energy in the Ferromagnetic 3d Metals. *Phys. Rev. Lett.* **1995**, *75*, 2871–2874.
22. Abe, H.; Miyawaki, J.; Sako, E.; Sakamaki, M.; Amemiya, K. Huge Perpendicular Magnetic Anisotropy of Fe Single Layer and Spin-Reorientation Transitions Observed in Fe/Co/Pd(111) Films. *Phys. Rev. B* **2008**, *78*, 014424.
23. Anisimov, A.; Farle, M.; Poulopoulos, P.; Platow, W.; Baberschke, K.; Isberg, P.; Wäppling, R.; Niklasson, A.; Eriksson, O. Orbital Magnetism and Magnetic Anisotropy Probed with Ferromagnetic Resonance. *Phys. Rev. Lett.* **1999**, *82*, 2390–2393.
24. Sjöstedt, E.; Nordström, L.; Gustavsson, F.; Eriksson, O. Uniaxial Magnetocrystalline Anisotropy of Metal/Semiconductor Interfaces: Fe/ZnSe(001). *Phys. Rev. Lett.* **2002**, *89*, 267203.
25. Burkert, T.; Nordström, L.; Eriksson, O.; Heinonen, O. Giant Magnetic Anisotropy in Tetragonal FeCo Alloys. *Phys. Rev. Lett.* **2004**, *93*, 027203.
26. Colarieti-Tosti, M.; Simak, S.; Ahuja, R.; Nordström, L.; Eriksson, O.; Åberg, D.; Edvardsson, S.; Brooks, M. Origin of Magnetic Anisotropy of Gd Metal. *Phys. Rev. Lett.* **2003**, *91*, 157201.
27. Andersson, G.; Burkert, T.; Warnicke, P.; Björck, M.; Sanyal, B.; Chacon, C.; Zlotea, C.; Nordström, L.; Nordblad, P.; Eriksson, O. Perpendicular Magnetocrystalline Anisotropy in Tetragonally Distorted Fe−Co Alloys. *Phys. Rev. Lett.* **2006**, *96*, 037205.
28. Yildiz, F.; Luo, F.; Tieg, C.; Abrudan, R. M.; Fu, X. L.; Winkelmann, A.; Przybylski, M.; Kirschner, J. Strongly Enhanced Orbital Moment by Reduced Lattice Symmetry and Varying Composition of $Fe_{1-x}Co_x$ Alloy Films. *Phys. Rev. Lett.* **2008**, *100*, 037205.
29. Yagi, Y.; Briere, T.; Sluiter, M.; Kumar, V.; Farajian, A.; Kawazoe, Y. Stable Geometries and Magnetic Properties of Single-Walled Carbon Nanotubes Doped with 3d Transition Metals: A First-Principles Study. *Phys. Rev. B* **2004**, *69*, 075414.
30. Escrig, J.; Landeros, P.; Altbir, D.; Vogel, E.; Vargas, P. Phase Diagrams of Magnetic Nanotubes. *J. Magn. Magn. Mater.* **2007**, *308*, 233–237.
31. Nosé, S. A Molecular Dynamics Method for Simulations in the Canonical Ensemble. *Mol. Phys.* **1984**, *52*, 255.
32. Kresse, G.; Hafner, J. *Ab Initio* Molecular Dynamics for Liquid Metals. *Phys. Rev. B* **1993**, *47*, 558–561.
33. Kresse, G.; Hafner, J. *Ab Initio* Molecular-Dynamics Simulation of the Liquid−Metal Amorphous-Semiconductor Transition in Germanium. *Phys. Rev. B* **1994**, *49*, 14251–14269.
34. Kresse, G., F. J. Efficiency of *ab Initio* Total Energy Calculations for Metals and Semiconductors Using a Plane-Wave Basis Set. *J. Comp. Mater. Sci.* **1996**, *6*, 15–50.
35. Kresse, G.; Furthmüller, J. Efficient Iterative Schemes for Ab Initio Total-Energy Calculations Using a Plane-Wave Basis Set. *Phys. Rev. B* **1996**, *54*, 11169–11186.
36. Blöchl, P. Projector Augmented-Wave Method. *Phys. Rev. B* **1994**, *50*, 17953–17979.
37. Kresse, G.; Joubert, D. From Ultrasoft Pseudopotentials to the Projector Augmented-Wave Method. *Phys. Rev. B* **1999**, *59*, 1758–1775.
38. Perdew, J.; Burke, K.; Ernzerhof, M. Generalized Gradient Approximation Made Simple. *Phys. Rev. Lett.* **1996**, *77*, 3865–3868.
39. Hobbs, D.; Kresse, G.; Hafner, J. Fully Unconstrained Noncollinear Magnetism within the Projector Augmented-Wave Method. *Phys. Rev. B* **2000**, *62*, 11556–11570.